Crystallographically Oriented Mesoporous WO 3 Films: Synthesis, Characterization, and Applications

ARTICLE *in* JOURNAL OF THE AMERICAN CHEMICAL SOCIETY · NOVEMBER 2001

Impact Factor: 12.11 · DOI: 10.1021/ja011315x · Source: PubMed

4 AUTHORS, INCLUDING:

Clara Santato
Polytechnique Montréal
61 PUBLICATIONS **1,927** CITATIONS
SEE PROFILE

Jan Augustynski
University of Geneva
111 PUBLICATIONS **3,987** CITATIONS
SEE PROFILE

Crystallographically Oriented Mesoporous WO_3 Films: Synthesis, Characterization, and Applications

Clara Santato, Marek Odziemkowski,† Martine Ulmann, and Jan Augustynski*

Contribution from the Department of Chemistry, University of Geneva, CH-1211 Geneva 4, Switzerland

Received May 30, 2001

Abstract: Mesoporous semiconducting films consisting of preferentially orientated monoclinic-phase nanocrystals of tungsten trioxide have been prepared using a novel version of the sol−gel method. Transformations undergone by a colloidal solution of tungstic acid, stabilized by an organic additive such as poly(ethylene glycol) (PEG) 300, as a function of the annealing temperature have been followed by means of a confocal Raman microscope. The shape and size of WO_3 nanoparticles, the porosity, and the properties of the films depend critically on preparation parameters, such as the tungstic acid/PEG ratio, the PEG chain length, and the annealing conditions. Well-crystallized WO_3 films combine excellent photoresponse to the blue region of the solar spectrum, up to 500 nm, with good transparency at wavelengths larger than 550 nm. Particular applications of these nanocrystalline WO_3 films include photoelectrochemical and electrochromic devices.

Introduction

Design and controlled growth of semiconductor nanostructures has become a rapidly expanding new field of materials chemistry.[1] Much of this work has focused on optically active II−VI and III−V semiconductors exhibiting quantum confinement effects.[2−4] In fact, the optical and electrical properties of the latter compounds strongly depend on the size and shape of the corresponding nanoparticles. Accordingly, the prospects of practical application in light-emitting-diodes[5a−c,e] and/or in biological labeling[5d,e] rely critically upon control of morphology and size distribution of the semiconductor nanoparticles.

On the other hand, studies pertaining to oxide semiconductor nanostructures are mainly aimed at the formation of high-surface-area, mesoporous, transparent films in view of their use in solar cells and/or in the field of photocatalysis.[6−11]

* To whom correspondence should be addressed.

† On leave from Department of Earth Sciences, University of Waterloo, Waterloo, Ontario, N2L 3G1, Canada.

(1) (a) Henglein, A. *Top. Curr. Chem.* **1988**, *143*, 113. (b) Wang, Y.; Herron, N. *J. Phys. Chem. B* **1991**, 95, 525. (c) Weller, H. *Adv. Mater.* **1993**, *5*, 88. (d) Weller, H. *Angew. Chem., Int. Ed. Engl.* **1993**, *32*, 41. (e) Alivisatos, A. P. *Science* **1996**, *271*, 933. (f) Alivisatos, A. P.; Barbara, P. F.; Castleman, A. W.; Chang, J.; Dixon, D. A.; Klein, M. L.; McLendon, G. L.; Miller, J. S.; Ratner, M. A.; Rossky, P. J.; Stupp, S. I.; Thompson, M. E. *Adv. Mater.* **1998**, *10*, 1297. (g) Brus, L. *J. Phys. Chem. Solids* **1998**, *59*, 459.

(2) (a) Brus, L. E. *J. Chem. Phys.* **1983**, *79*, 5566. (b) Rossetti, R.; Nakahara, S.; Brus, L. E. *J. Chem. Phys.* **1983**, *79*, 1086. (c) Fojtik, A.; Weller, H.; Koch, U.; Henglein, A. *Ber. Bunsen-Ges. Phys. Chem.* **1984**, *88*, 969. (d) Rossetti, R.; Ellison, J. L.; Gibson, J. M.; Brus, L. E. *J. Chem. Phys.* **1984**, *80*, 4464. (e) Finlayson, M. F.; Wheeler, B. L.; Kakuta, N.; Park, K. H.; Bard, A. J.; Fox, M. A.; Webber, S. E.; White, J. M. J. *Phys. Chem.* **1985**, *89*, 5676. (f) Spanhel, L.; Haase, M.; Weller, H.; Henglein, A. *J. Am. Chem. Soc.* **1987**, *109*, 5649. (g) Brennan, J. G.; Siegrist, T.; Carroll, P. J.; Stuczynski, S. M.; Reynders, P.; Brus, L. E.; Steigerwald, M. L. *Chem. Mater.* **1990**, *2*, 403. (h) Murray, C. B.; Norris, D. J.; Bawendi, M. G. *J. Am. Chem. Soc.* **1993**, *115*, 8706. (i) Chemseddine, A. *Chem. Phys. Lett.* **1993**, *216*, 265. (j) Vossmeyer, T.; Katsikas, L.; Giersig, M.; Popovic, I. G.; Diesner, K.; Chemseddine, A.; Eychmuller, A.; Weller, H. *J. Phys. Chem.* **1994**, *98*, 7665. (k) Rogach, A. L.; Katsikas, L.; Komowski, A.; Su, D. S.; Eychmuller, A.; Weller, H. *Ber. Bunsen-Ges. Phys. Chem.* **1996**, *100*, 1772. (l) Rogach, A. L.; Katsikas, L.; Komowski, A.; Su, S. D.; Eychmuller, A.; Weller, H. *Ber. Bunsen-Ges. Phys. Chem.* **1997**, *101*, 1668. (m) Peng, X. G.; Wickham, J.; Alivisatos, A. P. *J. Am. Chem. Soc.* **1998**, *120*, 5343. (n) Gao, M. Y.; Kirstein, S.; Mohwald, H.; Rogach, A. L.; Kornowski, A.; Eychmuller, A.; Weller, H. *J. Phys. Chem. B* **1998**, *102*, 8360. (o) Rogach, A. L.; Kornowski, A.; Gao, M. Y.; Eychmuller, A.; Weller, H. *J. Phys. Chem. B* **1999**, *103*, 3065. (p) Peng, X. G.; Manna, L.; Yang, W. D.; Wickham, J.; Scher, E.; Kadavanich, A.; Alivisatos, A. P. *Nature* **2000**, *404*, 59. (q) Mikulec, F. V.; Bawendi, M. G. *Mater. Res. Soc. Symp. Proc. (Nanophase and Nanocomposite Materials III)* **2000**, *581*, 139. (r) Eychmuller, A. *J. Phys. Chem. B* **2000**, *104*, 6514. (s) Peng, Z. A.; Peng, X. *J. Am. Chem. Soc.* **2001**, *123*, 1389. (t) Peng, Z. A.; Peng, X. *J. Am. Chem. Soc.* **2001**, *123*, 183.

(3) (a) Kortan, A. R.; Hull, R.; Opila, R. L.; Bawendi, M. G.; Steigerwald, M. L.; Carroll, P. J.; Brus, L. E. *J. Am. Chem. Soc.* **1990**, *112*, 1327. (b) Hoener, C. F.; Allan, K. A.; Bard, A. J.; Campion, A.; Fox, M. A.; Mallouk, T. E.; Webber, S. E.; White, J. M. *J. Phys. Chem.* **1992**, *96*, 3812. (c) Danek, M.; Jensen, K. F.; Murray, C. B.; Bawendi, M. G. *Appl. Phys. Lett* **1994**, *65*, 2795. (d) Mews, A.; Eychmuller, A.; Giersig, M.; Schoos, D.; Weller, H. *J. Phys. Chem.* **1994**, *98*, 934. (e) Hines, M. A.; Guyot-Sionnest, P. *J. Phys. Chem.* **1996**, *100*, 468. (f) Tian, Y.; Newton, T.; Kotov, N. A.; Guldi, D. M.; Fendler, J. H. *J. Phys. Chem.* **1996**, *100*, 8927. (g) Danek, M.; Jensen, K. F.; Murray, C. B.; Bawendi, M. G. *Chem. Mater.* **1996**, *8*, 173. (h) Peng, X. G.; Schlamp, M. C.; Kadavanich, A. V.; Alivisatos, A. P. *J. Am. Chem. Soc.* **1997**, *119*, 7019. (i) Dabbousi, B. O.; Rodriguez-Viejo, J.; Mikulec, F. V.; Heine, J. R.; Mattoussi, H.; Ober, R.; Jensen, K. F.; Bawendi, M. G. *J. Phys. Chem. B* **1997**, *101*, 9463.

(4) (a) Olshavsky, M. A.; Goldstein, A. N.; Alivisatos, A. P. *J. Am. Chem. Soc.* **1990**, *112*, 9438. (b) Uchida, H.; Curtis, C. J.; Nozik, A. J. *J. Phys. Chem.* **1991**, *95*, 5382. (c) Uchida, H.; Curtis, C. J.; Kamat, P. V.; Jones, K. M.; Nozik, A. J. *J. Phys. Chem.* **1992**, *96*, 1156. (d) Butler, L.; Redmond, G.; Fitzmaurice, D. *J. Phys. Chem.* **1993**, *97*, 10750. (e) Kher, S. S.; Wells, R. L. *Chem. Mater.* **1994**, *6*, 2056. (f) Micic, O. I.; Curtis, C. J.; Jones, K. M.; Sprague, J. R.; Nozik, A. J. *J. Phys. Chem.* **1994**, *98*, 4966. (g) Micic, O. I.; Sprague, J. R.; Curtis, C. J.; Jones, K. M.; Machol, J. L.; Nozik, A. J.; Giessen, H.; Fluegel, B.; Mohs, G.; Peyghambarian, N. *J. Phys. Chem.* **1995**, *99*, 7754. (h) Kher, S. S.; Wells, R. L. *Nanostruct. Mater.* **1996**, *7*, 591. (i) Guzelian, A. A.; Katari, J. E. B.; Kadavanich, A. V.; Banin, U.; Hamad, K.; Juban, E.; Alivisatos, A. P.; Wolters, R. H.; Arnold, C. C.; Heath, J. R. *J. Phys. Chem. B* **1996**, *100*, 7212. (j) Guzelian, A. A.; Banin, U.; Kadavanich, A. V.; Peng, X.; Alivisatos, A. P. *Appl. Phys. Lett.* **1996**, *69*, 1432.

(5) (a) Colvin, V. L.; Schlamp, M. C.; Alivisatos, A. P. *Nature* **1994**, *370*, 354. (b) Schlamp, M. C.; Peng, X. G.; Alivisatos, A. P. *J. Appl. Phys.* **1997**, *82*, 5837. (c) Rodriguez-Viejo, J.; Jensen, K. F.; Mattoussi, H.; Michel, J.; Dabbousi, B. O.; Bawendi, M. G. *Appl. Phys. Lett.* **1997**, *70*, 2132. (d) Bruchez, M.; Moronne, M.; Gin, P.; Weiss, S.; Alivisatos, A. *P. Science* **1998**, *281*, 2013. (e) Alivisatos, A. P. *Pure Appl. Chem.* **2000**, *72*, 3.

(6) (a) O'Regan, B.; Moser, J.; Anderson, M.; Grätzel, M. *J. Phys. Chem.* **1990**, *94*, 8720. (b) O'Regan, B.; Grätzel, M. *Nature* **1991**, *353*, 737. (c) Nazeeruddin, M. K.; Kay, A.; Rodicio, L.; Humphry, B. R.; Mueller, E.; Liska, P.; Vlachopoulos, N.; Grätzel, M. *J. Am. Chem. Soc.* **1993**, *115*, 6382. (d) Bach, U.; Lupo, D.; Comte, P.; Moser, J. E.; Weissortel, F.; Salbeck, J.; Spreitzer, H.; Grätzel, M. *Nature* **1998**, *395*, 583.

10.1021/ja011315x CCC: $20.00
Published on Web 10/06/2001

Most of the related work focused on the preparation of nanocrystalline titanium dioxide films following their successful application in dye-sensitized, liquid-junction solar cells.[6] Such films ca. 10 μm thick, formed by a network of interconnected colloidal particles, not only increase by a factor of almost 1000 the effective surface area over which a monolayer of photosensitive dye is adsorbed but also ensure an efficient collection of photogenerated electrons at the back contact. The latter requirement is particularly well fulfilled by nanocrystalline anatase films. Similar films, composed either of commercial P25 (anatase/rutile) nanoparticles ca. 25 nm in diameter or of smaller synthesized anatase particles, submitted to the band gap illumination, exhibit also an interesting photocatalytic activity for the photooxidation of organic compounds.[7] However, from the viewpoint of practical solar light applications, TiO_2 presents an intrinsic limitation due to its large band gap energy, 3.1 eV, covering only a marginal part of the solar spectrum. This is the reason for our and other groups' ongoing efforts intended to develop new nanostructured metal oxide materials with improved solar light absorption properties.

Here we describe the synthesis of nanostructured tungsten trioxide films exhibiting a series of interesting properties including high transparency for the wavelengths above 500 nm, excellent adherence to the conducting glass support, and large incident-light-to-current conversion efficiencies when acting as photoanodes in a photoelectrochemical cell. Due to their photoresponse extending to 500 nm (corresponding to a band gap energy of ca. 2.5 eV), these WO_3 photoanodes can operate under solar light illumination, delivering photocurrents in the range of a few milliamperes per square centimeter. In addition, a slightly modified preparation procedure allows formation of electrochromic windows having excellent long-term stability and high coloration efficiency.

The films were prepared by a kind of sol−gel process, using colloidal solutions of tungstic acid stabilized by addition of selected organic (poly)hydroxy compounds. The suitable choice of the precursor/stabilizer ratio and of the annealing conditions allows one to tailor the size of the resulting WO_3 nanoparticles and the film porosity. The latter features, together with the crystallinity of WO_3, are shown to affect critically the optical and photoelectrochemical properties of the films.[12]

Experimental Section

Preparation of Nanostructured WO_3 Films. Tungstic acid was obtained by passing an aqueous Na_2WO_4 solution through a proton exchange resin (Dowex 50 WX2-200, 100−200 mesh).[13] Tungstates are known to be easily protonated in aqueous solution and show a strong tendency to form polyoxoanions by oxygen bridging and release of water molecules.[14] The eluted solution was collected in ethanol under continuous magnetic stirring. Like a number of other solvents, ethanol tends to slow down the condensation of tungstic acid.[15] Following the elution, the solution was partially evaporated under reduced pressure to reach a concentration of ca. 0.5 mol/dm^3. An organic stabilizer (modulator) such as poly(ethylene glycol) (PEG) 300, glycerol, mannitol, or ethylene glycol was added to the freshly evaporated stirred

(7) (a) Vinodgopal, K.; Hotchandani, S.; Kamat, P. V. *J. Phys. Chem.* **1993**, *97*, 9040. (b) Bedja, I.; Hotchandani, S.; Kamat, P. V. *J. Phys. Chem.* **1994**, *98*, 4133. (c) Vinodgopal, K.; Stafford, U.; Gray, K. A.; Kamat, P. V. *J. Phys. Chem.* **1994**, *98*, 6797. (d) Wahl, A.; Ulmann, M.; Carroy, A.; Augustynski, J. *J. Chem. Soc., Chem. Commun.* **1994**, 2277. (e) Wahl, A.; Ulmann, M.; Carroy, A.; Jermann, B.; Dolata, M.; Kedzierzawski, P.; Chatelain, C.; Monnier, A.; Augustynski, J. *J. Electroanal. Chem.* **1995**, *396*, 41. (f) Vinodgopal, K.; Bedja, I.; Kamat, P. V. *Chem. Mater.* **1996**, *8*, 2180. (g) Bedja, I.; Kamat, P. V. *J. Phys. Chem.* **1995**, *99*, 9182. (h) Wahl, A.; Augustynski, J. *J. Phys. Chem. B* **1998**, *102*, 7820.

(8) (a) Duonghong, D.; Borgarello, E.; Grätzel, M. *J. Am. Chem. Soc.* **1981**, *103*, 4685. (b) Moser, J.; Grätzel, M. *J. Am. Chem. Soc.* **1983**, *105*, 6547. (c) Furlong, D. N.; Wells, D.; Sasse, W. H. F. *J. Phys. Chem.* **1986**, *90*, 1107. (d) Kormann, C.; Banhemann, D. W.; Hoffman, M. R. *J. Phys. Chem.* **1988**, *92*, 5196. (e) Hagfeldt, A.; Vlachopoulos, N.; Grätzel, M. *J. Electrochem. Soc.* **1994**, *141*, L82. (f) Joselevich, E.; Willner, I. *J. Phys. Chem.* **1994**, *98*, 7628. (g) Hagfeldt, A.; Grätzel, M. *Chem. Rev.* **1995**, *95*, 49. (h) Huang, S. Y.; Kavan, L.; Exnar, I.; Grätzel, M. *J. Electrochem. Soc.* **1995**, *142*, L142. (i) Moritz, T.; Reiss, J.; Diesner, K.; Su, D.; Chemseddine, A. *J. Phys. Chem. B* **1997**, *101*, 8052. (j) Elder, S. H.; Gao, Y.; Li, X.; Liu, J.; Mccready, D. E.; Windisch, C. F. *Chem. Mater.* **1998**, *10*, 3140. (k) Burnside, S. D.; Shklover, V.; Barbe, C.; Comte, P.; Arendse, F.; Brooks, K.; Grätzel, M. *Chem. Mater.* **1998**, *10*, 2419. (l) Rockenberger, J.; Scher, E. C.; Alivisatos, A. P. *J. Am. Chem. Soc.* **1999**, *121*, 11595. (m) Grätzel, M. *Curr. Opin. Colloid Interface Sci.* **1999**, *4*, 314. (n) Trentler, T. J.; Denler, T. E.; Bertone, J. F.; Agrawal, A.; Colvin, V. L. *J. Am. Chem. Soc.* **1999**, *121*, 1613. (o) Hagfeldt, A.; Grätzel, M. *Acc. Chem. Res.* **2000**, *33*, 269. (p) Vayssieres, L.; Hagfeldt, A.; Lindquist, S. E. *Pure Appl. Chem.* **2000**, *72*, 47. (q) Kavan, L.; Rathousky, J.; Grätzel, M.; Shklover, V.; Zukal, A. *J. Phys. Chem. B* **2000**, *104*, 12012. (r) Gomez, M. M.; Lu, J.; Olsson, E.; Hagfeldt, A.; Granqvist, C. G. *Sol. Energy Mater. Sol. Cells* **2000**, *64*, 385.

(9) (a) Nenadovic, M. T.; Rajh, T.; Micic, O. I.; Nozik, A. J. *J. Phys. Chem.* **1984**, *88*, 5827. (b) Judestein, P.; Livage, J. *J. Mater. Chem.* **1991**, *1*, 621. (c) Bedja, I.; Hotchandani, S.; Kamat, P. V. *J. Phys. Chem.* **1993**, *97*, 11064. (d) Bedja, I.; Hotchandani, S.; Carpentier, R.; Vinodgopal, K.; Kamat, P. V. *Thin Solid Films* **1994**, *247*, 195. (e) Hotchandani, S.; Bedja, I.; Fessenden, R. W.; Kamat, P. V. *Langmuir* **1994**, *10*, 1767. (f) Nishide, T.; Mizukami, F. *Thin Solid Films* **1995**, *259*, 212. (g) Nishide, T.; Yamaguchi, H.; Mizukami, F. *J. Mater. Sci. Lett.* **1995**, *30*, 4946. (h) Antonik, M. D.; Schneider, J. E.; Wittman, E. L.; Snow, K.; Vetelino, J. F. *Thin Solid Films* **1995**, *256*, 247. (i) Nishide, T.; Mizukami, F. *J. Mater. Sci. Lett.* **1996**, *15*, 1149. (j) Ulmann, M.; Santato, C.; Augustynski, J.; Shklover, V. *Electrode materials and processes for energy conversion and storage, IV*; McBreen, J., Mukerjee, S., Srinivasan, S., Eds.; Proceedings of the Electrochemical Society 97-13; Electrochemical Society: Pennington, NJ, 1997; p 328. (k) Pyper, O.; Schollhorn, R.; Donkers, J. J. T. M.; Krings, L. H. M. *Mater. Res. Bull.* **1998**, *33*, *1095*. (l) Ashrit, P. V.; Bader, G.; Trung, V. V. *Thin Solid Films* **1998**, *320*, 324. (m) Di Giulio, M.; Manno, D.; Micocci, G.; Serra, A.; Tepore, A. *J. Mater. Sci. Mater. Electron.* **1998**, *9*, 317. (n) Barton, D. G.; Shtein, M.; Wilson, R. D.; Soled, S. L.; Iglesia, E. *J. Phys. Chem. B* **1999**, *103*, 630. (o) Li, S. T.; Germanenko, I. N.; El-Shall, M. *S. J. Cluster Sci.* **1999**, *10*, 533. (p) Cantalini, C.; Atashbar, M. Z.; Li, Y.; Ghantasala, M. K.; Santucci, S.; Wlodarski, W.; Passacantando, M. J. *Vac. Sci. Technol. A* **1999**, *17*, 1873. (q) Bonhote, P.; Gogniat, E.; Grätzel, M.; Ashrit, P. V. *Thin Solid Films* **1999**, *350*, 269. (r) Sun, M.; Xu, N.; Cao, Y. W.; Yao, J. N.; Wang, E. G. *J. Mater. Res.* **2000**, *15*, 927. (s) Shiyanovskaya, I.; Hepel, M.; Tewksburry, E. *J. New Mater. Electrochem. Syst.* **2000**, *3*, 241. (t) Wang, H. L.; Lindgren, T.; He, J. J.; Hagfeldt, A.; Lindquist, S. E. *J. Phys. Chem. B* **2000**, *104*, 5686. (u) Santato, C.; Ulmann, M.; Augustynski, J. *Adv. Mater.* **2001**, *13*, 511. (v) Santato, C.; Ulmann, M.; Augustynski, J. *J. Phys. Chem. B* **2001**, *105*, 936.

(10) (a) Koch, U.; Fojtik, A.; Weller, H.; Henglein, A. *Chem. Phys. Lett.* **1985**, *122*, 507. (b) Vergés, M. A.; Mifsud, A.; Serna, C. J. *J. Chem. Soc., Faraday Trans.* **1990**, *86*, 959. (c) Spanhel, L.; Anderson, M. A. *J. Am. Chem. Soc.* **1991**, *113*, 2826. (d) Hoyer, P.; Eichberger, R.; Weller, H. *Ber. Bunsen-Ges. Phys. Chem.* **1993**, *97*, 630. (e) Hoyer, P.; Weller, H. *J. Phys. Chem.* **1995**, *99*, 14096. (f) Rensmo, H.; Keis, K.; Lindstrom, H.; Sodergren, S.; Solbrand, A.; Hagfeldt, A.; Lindquist, S. E.; Wang, L. N.; Muhammed, M. *J. Phys. Chem. B* **1997**, *101*, 2598. (g) Meulenkamp, E. A. *J. Phys. Chem. B* **1998**, *102*, 5566. (h) Keis, K.; Vayssieres, L.; Rensmo, H.; Lindquist, S. E.; A., H. *J. Electrochem. Soc.* **2001**, *148*, A149.

(11) (a) Bjorksten, U.; Moser, J.; Grätzel, M. *Chem. Mater.* **1994**, *6*, 858. (b) Khan, S. U. M.; Akikusa, J. *J. Phys. Chem. B* **1999**, *103*, 7184. (c) Beermann, N.; Vayssieres, L.; Lindquist, S. E.; Hagfeldt, A. *J. Electrochem. Soc.* **2000**, *147*, 2456.

(12) The sol−gel route has been employed by several authors for the deposition of thin WO_3 films principally in view of electrochromic applications.[32] Tungstic acid, peroxotungstic acid, and tungsten alkoxides have been used as the precursors. There is only a single report in the literature regarding photoelectrochemical properties of such films. The latter authors[9t] essentially followed the preparation method of the WO_3 films described in our short earlier publication.[9j]

(13) (a) Richardson, E. *J. Inorg. Nucl. Chem.* **1959**, *12*, 79. (b) Chemseddine, A.; Morineau, R.; Livage, J. *Solid State Ionics* **1983**, *9*, 357. (c) Chemseddine, A.; Henry, M.; Livage, J. *Rev. Chim. Miner.* **1984**, *21*, 487.

(14) (a) Cotton, F. A.; Wilkinson, G. *Advanced Inorganic Chemistry*, 3rd ed.; Interscience Publishers: New York, 1972. (b) Pope, M. T. In *Comprehensive Coordination Chemistry*; Wilkinson, G., Gillard, R. D., McCleverty, J. A., Eds.; Pergamon Press: New York, 1987; Vol. 3. (c) Hastings, J. J.; Howarth, O. W. *J. Chem. Soc., Dalton Trans.* **1992**, 209. (d) Cruywagen, J. J. In *Advances in Inorganic Chemistry*; Sykes, A. G., Ed.; Academic Press: New York, 1999; Vol. 49.

(15) Lemerle, J.; Lefebre, J. *Can. J. Chem.* **1977**, *55*, 3758.

solution. Compounds of this kind are known to form complexes with tungsten oxoanions.[13a,14a] A typical WO_3/organic stabilizer ratio was 0.5 w/w. The obtained relatively viscous, pale yellow solution (maintained under continuous stirring) was normally used for the formation of WO_3 films for no more than 3 days. It is important to note that if no organic stabilizer was included, the freshly eluted solution of tungstic acid became highly viscous and opaque after a few hours and within 1 day formed a dense yellow precipitate.

The WO_3 films were prepared by spreading a portion of colloidal solution onto conducting glass substrates comprising a 0.5 μm thick overlayer of F-doped SnO_2 (Libbey Owens Ford, 12 Ω/square). The deposited layer was first dried at room temperature for 10 min and then annealed in flowing oxygen at 400−550 °C for 30 min. The thickness of individual WO_3 layers was ca. 0.4 μm; thicker films were obtained by consecutive applications of the solution, each followed by the annealing. For comparison purposes, a series of samples were also prepared (following the same procedure) using a dispersion of tungstic acid without any organic additive.

Techniques. Raman spectra were obtained with a Labram I microscope system with an air-cooled CCD detector (1024 × 256 pixel) using a 20 mW HeNe (632.8 nm) laser in the backscattering geometry. The instrument is equipped with a stigmatic spectrometer including two interchangeable holographic gratings, 600 and 1800 grooves/mm. The latter grating and a 100 μm open entrance slit were used in this work, giving the spectra resolution of ca. 2 cm^{-1}. The optical throughput is better than 30%, resulting in the high sensitivity. All Raman spectra were obtained using a 100× magnification Olympus objective. Due to the nature of tungsten oxide films (see explanation in the Results and Discussion), the instrument was used in the confocal mode of operation. Such a mode of operation was achieved by closing the confocal pinhole to 200 or 50 μm. The optical alignment of the instrument was optimized using a 520 cm^{-1} Raman signal of a silicon wafer. For the 100× magnification lens, the confocal pinhole setting at 200 and 50 μm resulted in 3 and 1.2 μm sampling depths, respectively. In this situation, the analyzed surface is perfectly defined with precision of 0.1 μm, and for nearly transparent films such as WO_3 films[16] this means that the analyzed volume is defined and controlled. Furthermore, in the backscattering, undesirable fluorescence is minimized. Two kinds of classic experiments possible with the confocal Raman spectroscopy, i.e., the "particle in the matrix" and the "multilayer laminate", were performed. The former case involves analysis of discontinuous or defected WO_3 films (particles) deposited on the conducting glass (matrix). The latter case is the analysis of the continuous, not defected, WO_3 films coated on the conducting glass; here, in fact, we deal with the three-layer "laminate" consisting of glass, F-doped SnO_2 film, and the WO_3 film. Each Raman measurement was followed by collection of a white light image of the analyzed sample area. Laser power had to be adjusted specifically to the nature of the sample and is indicated in the figure captions. The laser power was adjusted by changing the filter density and was always measured at the sample surface, i.e., under the microscope.

Thermogravimetric/differential thermal analyses were performed using a TGA/DC 320 Seiko instrument.

X-ray diffraction patterns were recorded on a Scintag powder diffractometer equipped with a Ge detector and on a STOE automated system equipped with a small position-sensitive detector. Cu Kα radiation was used (λ = 1.5406 nm).

Grazing incidence synchrotron X-ray measurements were performed using a Huber powder diffractometer on the beam line B2 of HASYLAB (Hamburg, Germany). Scanning electron microscopy (SEM) images were taken at 30 kV accelerating voltage in a Hitachi S-900 "in-lens" field-emission scanning electron microscope with a standard Everhard-Thornley SE detector and a YAG-type BSE detector.

Atomic force microscopy images were obtained in an air AFM/STM Auto Probe CP Research, from Thermo Microscopes, using Si cantilevers. Images were taken in a noncontact AFM mode.

HRTEM studies of WO_3 nanopowders were performed at 300 kV in a Philips CM 30 ST transmission electron microscope.

UV−vis transmission spectra were recorded on a Cary 500 model 8.01 spectrophotometer equipped with an integrating sphere. Accordingly, we collected the light transmitted in all directions (total transmittance). For these experiments, the WO_3 films were deposited on small fused silica plates.

The films were tested for their photoelectrochemical activity in a two-compartment Teflon cell equipped with a quartz window, by illuminating the WO_3 electrode from the side of the film/solution interface. A platinum counter-electrode (large area Pt grid) was separated from the WO_3 film electrode by a Nafion membrane. The potential of the WO_3 electrode was monitored versus a mercurous sulfate/mercury reference electrode. The WO_3 films were illuminated with the simulated solar AM 1.5 light obtained using a 150 W xenon lamp equipped with a Schott 113 filter and neutral density filters. The wavelength photoresponse (i.e., incident photon-to-current conversion efficiency vs excitation wavelength) of the WO_3 electrodes was determined using a 500 W xenon lamp (Ushio UXL-502HSO) set in an Oriel model 66021 housing and a Multispec 257 monochromator (Oriel) with a bandwidth of 4 nm. The absolute intensity of the incident light from the monochromator was measured with a model 730 A radiometer/photometer from Optronic Lab. The photoelectrochemical measurements were carried out at ca. 25 °C under potential-controlled conditions. Chemicals used in the present work were obtained from Fluka and Merck and were of the highest available purity.

Results and Discussion

We selected the organic additives used for the synthesis of nanostructured WO_3 films, i.e., poly(ethylene glycol) (PEG) 300, glycerol, mannitol, and ethylene glycol, according to the following three criteria: adherence, homogeneity, and transparency of the resulting film. All of these films annealed at 550 °C were light yellow and exhibited excellent adherence to the conductive glass support and either excellent or good homogeneity and transparency. Subsequent comparison of the photoelectrochemical activities of those films clearly designated PEG 300 as the most effective organic additive. The possible reasons for this strong varying photoactivity are discussed below in connection with the corresponding SEM images. Consequently, further detailed investigations were mainly focused on the WO_3 films prepared using PEG 300 as the additive.

Raman Spectra. Raman measurements were first conducted for a series of films obtained using a colloidal solution of tungstic acid free of PEG, annealed at increasing temperatures. White light images of the coated conducting glass samples are presented in Figure 1. Excluding uncoated areas of the substrate, three arbitrarily chosen locations on each image were subjected to Raman analysis. The coatings prepared in the absence of PEG were characterized by randomly distributed shiny particulates. Focusing the laser microprobe on the gray area resulted in a Raman spectrum of glass with typical very broad bands around 470 and 1100 cm^{-1}. The spectra exhibiting the best signal-to-noise (S/N) ratio are presented in Figure 2 as a function of the thermal treatment. Two asymmetric peaks at 663 and 952 cm^{-1} characterize the Raman spectrum of the sample annealed at 100 °C. The band around 950 cm^{-1} is assigned to the stretching mode of the terminal W═O bond; this mode is common for all types of tungsten trioxide hydrates. Following the vibration assignments by Daniel et al.,[17] the band at 663 cm^{-1} should be attributed to stretching O−W−O modes of the bridging oxygens. However, the spectrum of the sample annealed at 100 °C cannot be attributed to any specific form of hydrate; it rather resembles both in the band shape and relative intensities that of the so-called xerogel obtained by the ion-exchange method.[18,19] With

(16) von Rottkay, K.; Rubin, M.; Wen, S. J. *Thin Solid Films* **1997**, *306*, 10.

(17) Daniel, M. F.; Desbat, B.; Lassegues, J. C.; Gerand, B.; Figlarz, M. *J. Solid State Chem.* **1987**, *67*, 235.

(18) Nanba, T.; Nishiyama, Y.; Yasui, I. *J. Mater. Res.* **1991**, *6*, 1324.

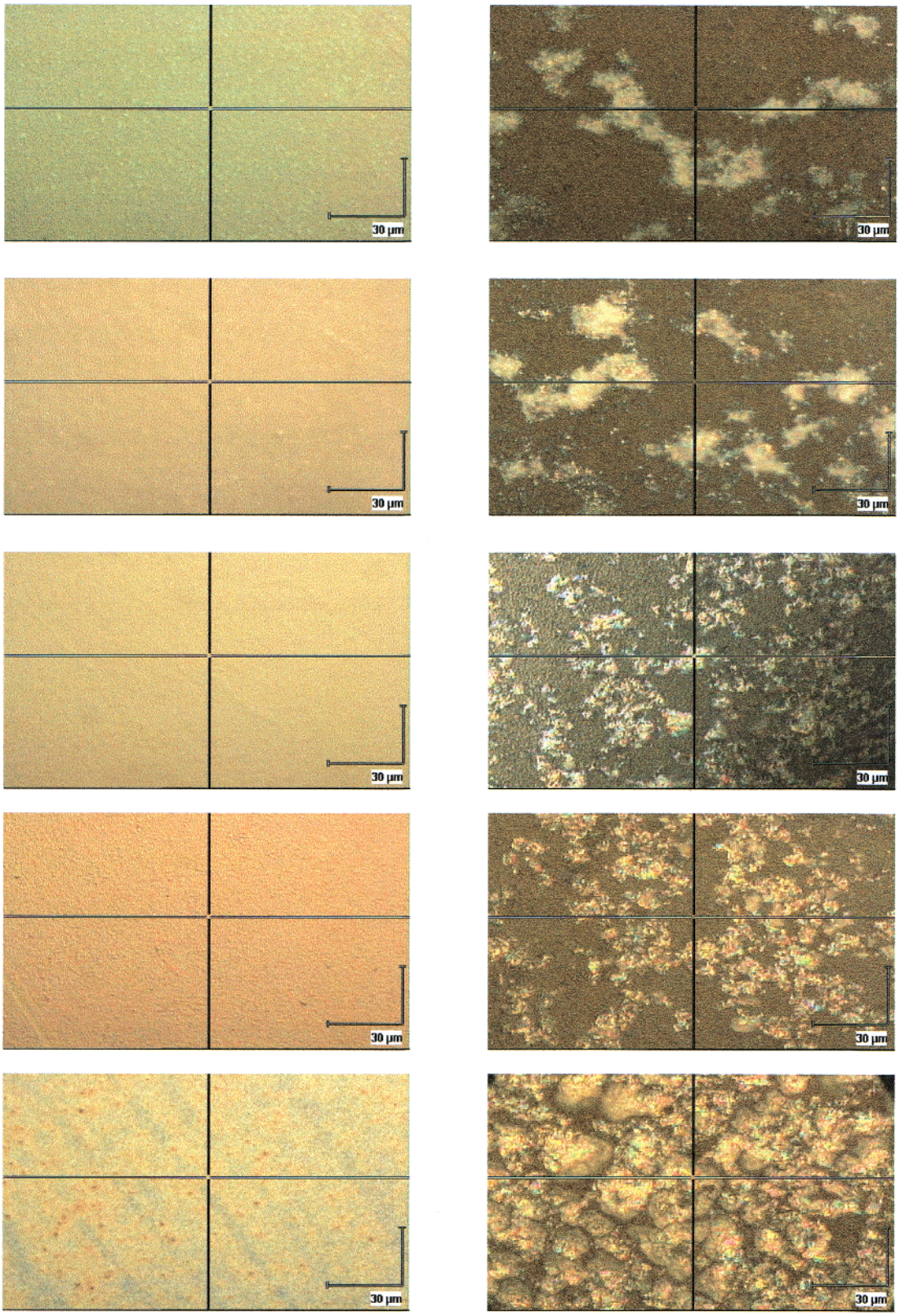

Figure 1. White light images of a series of colloidal WO_3 films deposited on conducting glass substrates; magnification 100×. The films were annealed at increasing temperatures (from the bottom to the top): 100, 200, 300, 400, and 500 °C. On the left-hand side of the figure are represented films prepared from a tungstic acid/PEG 300 solution, on the right-hand side those obtained using a tungstic acid solution without an additive.

the increase of annealing temperature to 200 °C, Raman bands shifted to higher wavenumber and became broader. The spectrum again cannot be assigned to any specific crystalline tungsten oxide or hydrated oxide.[17] Evidently, this spectrum has all the characteristics of an amorphous tungsten oxide (a-WO_3), namely all bands are broad and their relative band intensities are characteristic of a-WO_3.[18,20,21] The band at around 960 cm^{-1} again can be assigned to the terminal W═O stretching mode, possibly on the surface of the cluster and in microvoid structures in the film.[20,22] The broad band centered at ca. 760 cm^{-1} most probably can be deconvoluted into several Raman peaks, including the strongest peaks at 715 and 807 cm^{-1} of a

monoclinic WO_3. Indeed, these well-defined peaks began to be visible for the films treated at 300 and 400 °C. As shown in Figure 2, the increase of annealing temperature to 300 °C resulted in the decreased intensity of the stretching mode of the terminal W═O bond at ∼950 cm^{-1}, with the simultaneous appearance of new bands at ∼270, 702, and 803 cm^{-1}. The spectrum of the sample treated at 400 °C was very strong, with well-defined Raman bands at 272, 322, 709, and 807 cm^{-1}. These bands fall very close to the wavenumbers of the four strongest modes of monoclinic tungsten oxide (*m*-WO_3).[17] The bands at 272 and 322 cm^{-1} correspond to O−W−O bending modes of the bridging oxygen,[17] and the bands at 709 and 807 cm^{-1} are the corresponding stretching modes. The exception is a shoulder at 640 cm^{-1} which cannot be assigned to *m*-WO_3. We attribute this shoulder to the O−W−O stretching vibration of the bridging oxygen in the residual hydrated tungsten oxide, since very similar bands were observed for $WO_3 \cdot H_2O$.[17] This assignment is tentative and requires further confirmation by IR measurements. It has, however, further support in the fact that we also observed a residual weak signal of terminal W═O which is exclusively characteristic of hydrated oxides. The spectrum of the film treated at 500 °C is free of the shoulder at ca. 640 cm^{-1}; however, the band at 709 cm^{-1} is still asymmetric. The spectrum has typical bands of the crystalline WO_3, namely weak bands at around 430 and 450 cm^{-1} are visible. These bands, already perceptible in the spectrum of the film annealed at 400 °C, together with the lattice modes below 200 cm^{-1} are characteristic of crystalline tungsten oxides.[23] In this work, due to the notch filter cutoff, the lattice vibrations could not be investigated.

In summary, it can be said that, through the thermal treatment, the xerogel was transformed into *a*-WO_3 at 200 °C and further into a crystalline oxide, which only resembles the monoclinic form of WO_3. Note that the bands observed in the sample treated at 500 °C did not fall exactly at frequencies of the monoclinic WO_3; furthermore, the recorded spectra had a tendency to shift, with a dependence on the illuminated spot. This discrepancy might have its origin in the unknown crystal imperfections or might simply arise from a varying orientation of this polycrystalline material toward the polarized laser beam.

A similar Raman spectroscopic study was also performed on a series of films prepared from tungstic acid/PEG 300 colloidal solution (corresponding to a 0.5 w/w WO_3/PEG ratio). White light images of the coated conducting glass samples are displayed in Figure 1. The coatings prepared in the presence of PEG were almost perfectly uniform. The images presented here should be considered as the worst ones. These particular areas were chosen for two reasons only: namely to make the focusing of the microscope easier (at a 100× magnification, the microscope depth of field is very small) and to check the visible imperfections for chemical homogenity/heterogenity in comparison with an average area of the sample. The average areas plus all visible imperfections in the image were subjected to Raman analysis. When the Raman microprobe was focused, these visual imperfections as well as the average area gave almost identical Raman spectra responses, which differ only in the intensity and the S/N ratio. Figure 3 shows spectra of the deposited films heat-treated at several temperatures. The Raman spectra recorded for samples annealed at lower temperatures are characterized by lower S/N ratios than their counterpart samples free of PEG. In the case of many samples treated at low temperatures, we had to use extremely low laser power (i.e., 1.23 mW or even 0.132 mW) to avoid sample modification. Note that, for the Raman microscope employed in this study, the powers of 1.23 and 0.132 mW translate to power density at the sample surface of 39.5 and 4.24 W/cm^2, respectively.

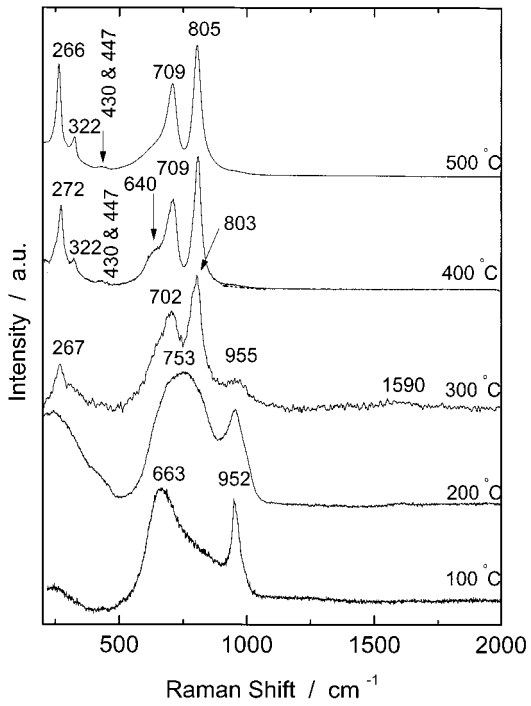

Figure 2. Comparison of Raman spectra for the WO_3 films deposited on the conducting glass substrates using a tungstic acid solution. The spectra of the films annealed at 100 and 200 °C were obtained using laser power of 0.132 mW, accumulation time 20 s, 10 accumulations. Raman spectra of the films annealed at 300, 400. and 500 °C were obtained using a laser power of 1.23 mW, accumulation time 10 s, 10 accumulations.

The Raman spectrum of the sample annealed at 100 °C is characterized by a symmetric broad band at 643 cm^{-1}, followed by a strong band at 965 cm^{-1} and a shoulder at 986 cm^{-1}. The former band should be assigned to the stretching O−W−O vibration of the bridging oxygen,[17] while the bands at higher wavenumbers are assigned, respectively, to the symmetric and asymmetric stretching of terminal W═O.[13c] However, there is still a possible alternative assignment for the shoulder at 986 cm^{-1}. Infrared studies of $MoO_3 \cdot 2H_2O$ and $WO_3 \cdot 2H_2O$ predict the existence of four terminal metal═O groups in the unit cell, with four distinct lengths of metal═O bonds.[17] Therefore, the band at 986 cm^{-1} might be alternatively assigned to a shorter terminal W═O bond. Chemseddine et al.[13c] observed an almost identical Raman spectrum as a result of the polycondesation of tungsten anions in the presence of acetone as an organic additive. Following the latter authors,[13c] we can consider that at 100 °C we deal with a xerogel. From comparison with the xerogel obtained in the absence of organic additive (see Figure 2), it can be claimed that upon addition of PEG the O−W−O bond becomes weaker and the W═O bond stronger. After annealing at 200 °C, several new Raman bands became visible at 244, 322, 697, 787, and 820 cm^{-1}. Following the work by Daniel et al.,[17] the majority of the bands (i.e., 244, 322, 645, 697, and 820) can be assigned to a metastable hexagonal tungsten trioxide

(19) Nonaka, K.; Takase, A.; Miyakawa, K. *J. Mater. Sci. Lett.* **1993**, *12*, 274.
(20) Lee, S.-H.; Cheong, H. M.; Zhang, J.-G.; Mascarenhas, A.; Benson, D. K.; Deb, S. K. *Appl. Phys. Lett.* **1999**, *74*, 242.
(21) Lee, S.-H.; Cheong, H. M.; Tracy, C. E.; Mascarenhas, A.; Czanderna, A. W.; Deb, S. K. *Appl. Phys. Lett.* **1999**, *75*, 1541.
(22) Gabrusenok, E. V.; Cikmacs, P.; Lusis, A.; Kleperis, J.; Ramans, G. M. *Solid State Ionics* **1984**, *14*, 25.
(23) Takase, A.; Miyakawa, K. *Jpn. J. App. Phys.* **1991**, *30*, L1508.

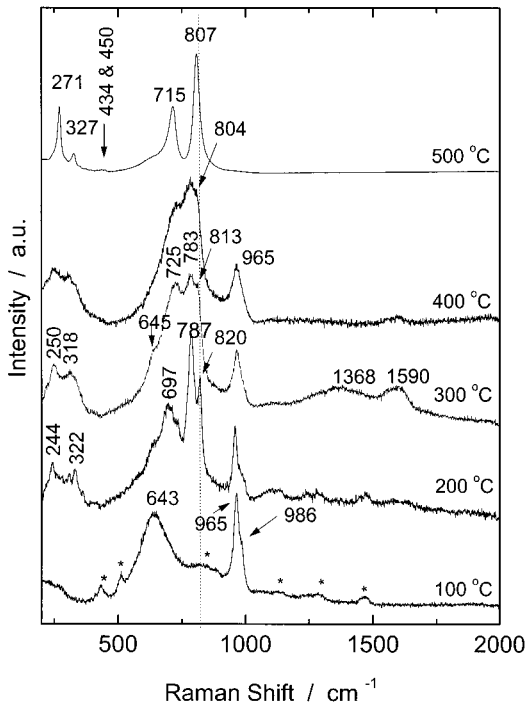

Figure 3. Comparison of Raman spectra for a series of WO_3 films formed on conducting glass substrates using a tungstic acid/PEG 300 solution. The spectra of the films annealed at 100, 200, and 300 °C were obtained using laser power of 0.132 mW, accumulation time 20 s, 20 accumulations. Raman spectra of the films annealed at 400 °C were obtained using laser power of 1.23 mW, accumulation time 20 s, 10 accumulations. The bands corresponding to the organic additive are indicated with asterisks.

(*h*-WO_3). The presence of an additional band at 787 cm^{-1} and particularly of bands at 965 and 986 cm^{-1} indicates that the analyzed material still contains an unknown form of hydrated WO_3. Further increase of the annealing temperature to 300 °C caused a decrease in intensity of the stretching mode of terminal W═O bond at ca. 965 cm^{-1}, with the simultaneous appearance of new bands at ∼1368 and ∼1590 cm^{-1}. The latter bands can be attributed to the disordered graphitic carbon.[24] It is interesting to note, in this connection, that the broad band at ∼1368 cm^{-1} tailing toward lower wavenumbers is typical of an incomplete combustion of organic matter.[25] Importantly, for the latter sample, at least few bands (i.e., 250, 318, 645, and 813 cm^{-1}) of *h*-WO_3 are still persistent. The overall shape of the Raman spectrum recorded for the film annealed at 400 °C did not change, the exceptions being the strongly decreased bands of disordered graphitic carbon. The second small change regarded the frequency of the 813 cm^{-1} band which shifted to 804 cm^{-1}. The spectrum of the sample annealed at 500 °C is presented as the upper curve of Figure 3. These bands fall exactly at wavenumbers of the fundamental modes of *m*-WO_3.[17] The spectrum has also characteristic bands of the crystalline tungsten oxide,[23] namely weak bands around 430 and 450 cm^{-1} are visible. It should be noted that as many as five different sample locations were investigated, and the obtained spectra were identical (as far as resolution of the instrument is concerned, i.e., 2 cm^{-1}). This excellent agreement with the literature data for *m*-WO_3 might suggest a single preferential orientation of the microcrystalline material.

(24) Kraft, T.; Nickel, K. G. *J. Mater. Chem.* **2000**, *10*, 671. McCreery, R. L. In *Electroanalytical Chemistry*; Bard, A. J., Ed.; 1991; Vol. 17, p 221.

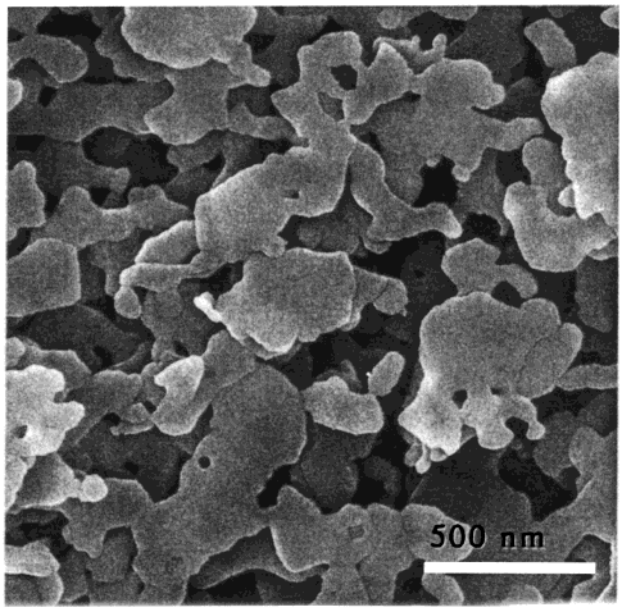

Figure 4. Scanning electron microscopy image of a WO_3 film obtained by the application of a colloidal solution of tungstic acid and annealing at 550 °C.

The above-discussed Raman data show clearly that the addition of PEG to the colloidal solution of tungstic acid strongly affects the process of the subsequent WO_3 film formation occurring during the heat treatment. In particular, the presence of PEG induces formation of the metastable hexagonal tungsten trioxide (*h*-WO_3) as an intermediate state at 200 °C, while, under the same conditions, the tungstic acid gel without PEG is transformed into amorphous WO_3. In addition, the film prepared from the gel including PEG apparently retains water in the structure of WO_3 even at 400 °C, the strong stretching mode of terminal W═O bond being the evidence. Importantly, the presence of PEG in the gel shifts its definite conversion into the monoclinic form of WO_3 to higher temperatures. As a matter of fact, the evidence for the crystalline *m*-WO_3 was observed only for the film annealed at 500 °C although, in the absence of PEG, weak Raman signals at 430 and 447 cm^{-1}, attributable to the crystalline WO_3, were already present in the spectrum of the film annealed at 400 °C.

TG/DTA. Complementary information regarding the thermal behavior of PEG 300 and the way in which it affects the crystallization of WO_3 films was obtained from a series of TG/DTA measurements. Pyrolysis of the PEG 300 polymer alone occurs in the range of 190−240 °C and is accompanied by one sharp and a second, much weaker, exothermic peak. When PEG 300 forms a mixture with tungstic acid, the two above peaks are shifted to a higher range of temperatures (260−320 °C); simultaneously, there is a change in their intensity ratio. Such a strong increase of the thermal stability of PEG 300 supports the idea of its covalent bonding to tungstic acid persisting with hydrated WO_3. The DTA plot recorded for a tungstic acid/PEG 300 mixture exhibits also an additional weak exothermic peak at 360 °C which we attribute to the conversion of metastable *h*-WO_3 into *m*-WO_3. This is supported by the results of XRD experiments, performed as a function of the increasing sample temperature, which indicated appearance of the diffraction peaks characteristic of the monoclinic form of WO_3 from 360 °C.

SEM. In Figure 4 is shown scanning electron micrograph (a top view) of a WO_3 film deposited using a solution of tungstic

(25) Odziemkowski, M.; Koziel, J.; Irish, D. E.; Pawliszyn, J. *Anal. Chem.* **2001**, *73*, 3131.

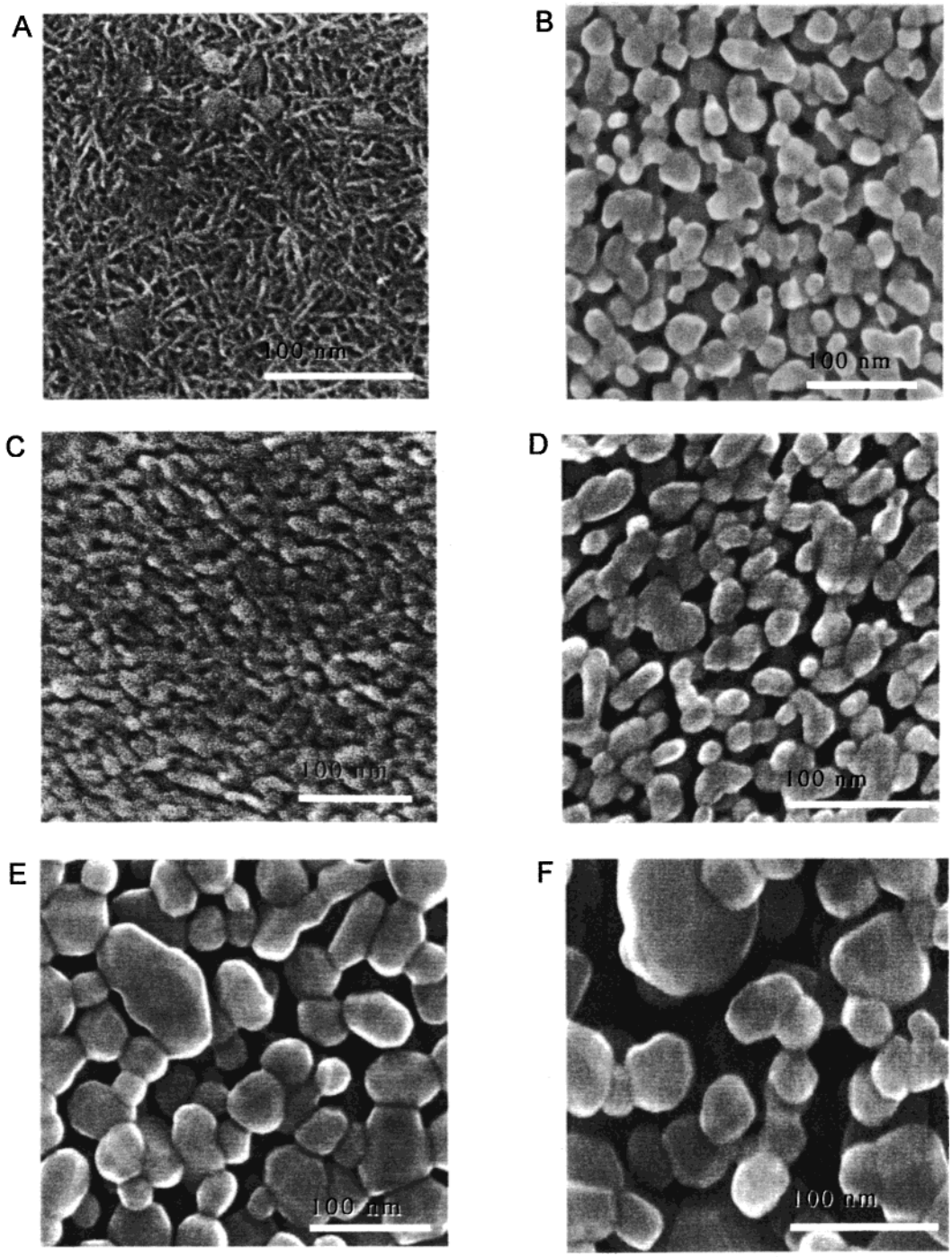

Figure 5. Series of scanning electron micrographs of WO_3 films prepared by the deposition of a tungstic acid/PEG 300 colloidal solution and annealing (A) at 400 °C for 30 min, (B) at 400 °C for 10 h, (C) at 450 °C for 30 min, (D) at 500 °C for 30 min, (E) at 550 °C for 30 min, and (F) at 600 °C for 30 min.

acid without any organic additive, annealed for 30 min at 550 °C (the latter heat-treatment conditions result in an optimum photoactivity for this kind of films). The film is composed of relatively large, about 400 × 200 nm sized, irregular plate-like particles and exhibits substantial porosity.

Morphological changes occurring in the WO_3 films, prepared using the standard tungstic acid/PEG 300 colloidal solution, as a function of the annealing temperature are illustrated by a series of SEM images in Figure 5. In the range of the investigated heat-treatment temperatures, from 400 to 600 °C, the WO_3 films reach mechanical stability, allowing their utilization in photoelectrochemical and/or electrochromic devices. All the films displayed in Figure 5 were formed by a single application of the colloidal solution followed by an annealing for 30 min at a given temperature. The sample heated at 400 °C consisted of a network of ca. 30 nm long needle-like particles. In addition, isolated spherical particles are also perceptible in Figure 5A. In the film annealed at 450 °C, the fibers are replaced by small (ca. 15 nm wide) plate-like particles (Figure 5C). Further increasing the annealing temperature to 500 °C rendered the film porous; most of the plate-like particles have sizes in the range of 10−30 nm (Figure 5D). One possible reason for the large increase of film porosity, occurring between 400 and 500 °C, might be retention of some organic moieties after removal of PEG 300 by pyrolysis. As an indirect evidence one can mention, in this connection, the persistence in the Raman

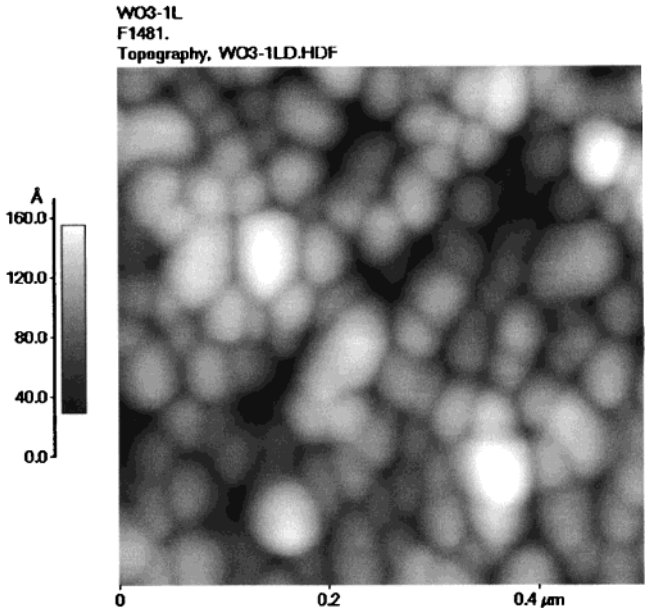

Figure 6. Topographical AFM image of a WO_3 film similar to that in Figure 5E deposited on a fused silica substrate.

spectrum of the film annealed at 400 °C (Figure 3) of weak signals of graphitic carbon attributable to an incomplete combustion of the organic matter. However, evident also is a significant film sintering occurring at 500 °C and continuing at higher temperatures, resulting in an increase of the particle's size and of the film porosity (Figures 5E,F). Taking into account a relatively short duration (i.e., 30 min) of the regular annealing to which we submitted the WO_3 films, some samples underwent prolonged heat treatments. For example, annealing at 400 °C for 10 h resulted in a substantially changed film morphology with the formation of a regular network of small plate-like particles (Figure 5B).

AFM. To gain more insight into the morphology of the WO_3 films, a few samples were also examined by atomic force microscopy. These samples, annealed at 550 °C, were deposited on fused silica substrates. Figure 6 shows a topographical AFM image of a ca. 0.4 μm thick film obtained by a single application of the tungstic acid/PEG 300 solution. Like other thicker samples prepared under similar conditions, the film represented in Figure 6 appears very smooth, with the maximum protuberance lower than 16 nm.

XRD. X-ray diffraction (XRD) patterns of the above films, shown in Figure 7, are consistent with increases both in the size of nanocrystals and in the crystallinity of WO_3 with increasing annealing temperature. The XRD spectrum of the sample heated at 400 °C exhibits a broad peak centered at ca. 23° and a series of peaks (indicated with asterisks) originating from the SnO_2 underlayer. Annealing the film at 450 °C resulted in the appearance of two sharp peaks at 23.5° (having a shoulder on the small angles side) and 24° (Figure 7B). Further increase of heat-treatment temperature to 550 °C led to an evident improvement of the crystallinity of the film, as indicated by a strong increase in the intensity of the principal peaks in Figure 7C. In addition, a third sharp peak became clearly perceptible in the 22−25° region of the latter XRD spectrum The XRD pattern of a WO_3 film annealed at 550 °C and then removed from the support, measured in a capillary in transmission mode, could be indexed on the monoclinic unit cell ($a = 7.298(7)$ Å, $b = 7.534(5)$ Å, $c = 7.679(8)$ Å, $\beta = 90.6(1)°$). In view of the results of XRD measurements suggesting preferential orientation of WO_3 nanocrystallites in the film annealed at 550 °C (cf.

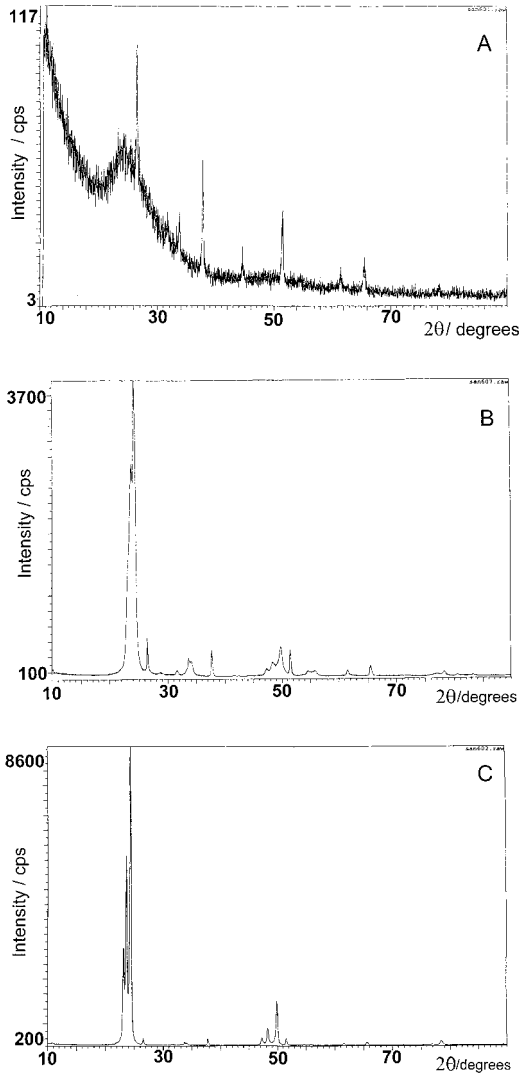

Figure 7. X-ray diffraction data for the WO_3 films represented in Figure 5 and annealed (A) at 400 °C, (B) at 450 °C, and (C) at 550 °C.

Figure 7C), it became important to check whether such a specific orientation was preserved across the whole film. For those grazing incidence X-ray diffraction experiments, we used thicker WO_3 films deposited on glass (without a SnO_2 overlayer). In such a way, we wanted to rule out any doubt about a possible epitaxial growth of the WO_3 film which could be induced by the underlayer of nanocrystalline SnO_2. The films were formed by subsequent deposition and annealing at 550 °C of three layers of the tungstic acid/PEG 300 colloidal solution. Diffraction patterns of these films, obtained using a synchrotron radiation, showed strong preferential orientation of the 200, 020, and 002 faces of WO_3 crystallites parallel to the substrate (cf. Figure 8A). Measurements involving variation of the glancing angle of incident radiation demonstrated that the intensity ratio of the principal diffraction peaks remained essentially the same (Figure 8B) for the angles decreasing from 5 to 0.5°. This confirms the possibility of building relatively thick crystallographically orientated WO_3 films using the sequential deposition/annealing method described here.

Photoelectrochemistry. In an attempt to establish a correlation between the structure and morphology of WO_3 films and their photoelectrochemical activity, we tested a large number of samples prepared using various organic additives and annealed over a broad range of temperatures. We included also in this comparison some samples which did not fulfill com-

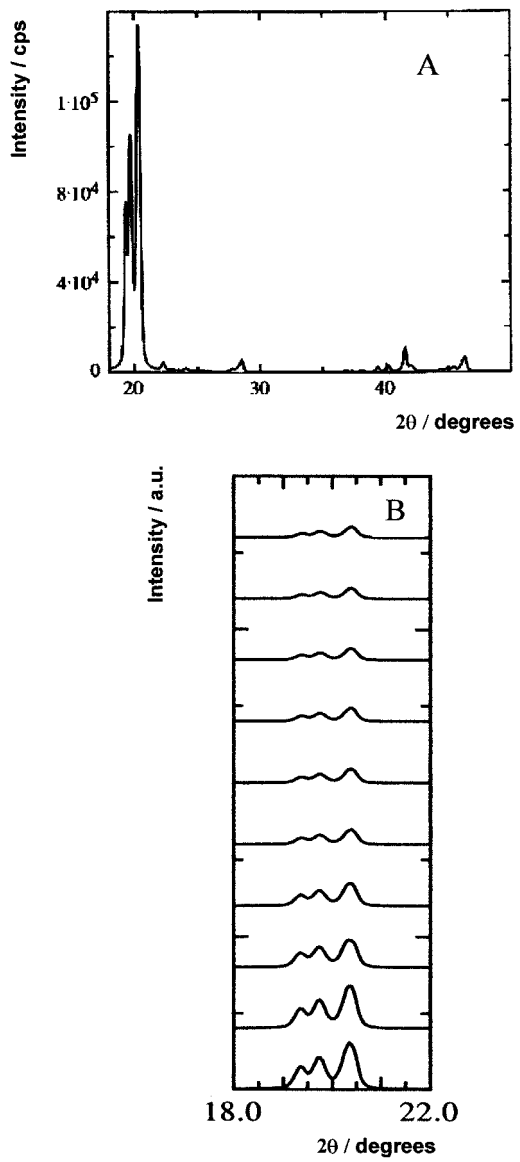

Figure 8. (A) Diffraction pattern of a ca. 1.2 μm thick WO_3 film deposited on glass using a tungstic acid/PEG 300 solution and annealed at 550 °C (λ = 1.294 Å, synchrotron radiation, $\theta/2\theta$ scan). Sharp diffraction peaks correspond, from left to right, to 002, 020, and 200 faces of WO_3 crystallites. (B) Diffraction patterns of the same WO_3 film recorded at decreasing glancing angles, from $\alpha = 5°$ (bottom) to 0.5° (top).

pletely the criteria of excellent transparency and adherence to the substrate. Since the photoresponse of nanostructured WO_3 films (at least those exhibiting the monoclinic structure) extends to 500 nm,[9u,v] all samples were tested under simulated solar AM 1.5 illumination. In Figure 9 are displayed photocurrent−voltage plots for a series of WO_3 films deposited using the standard tungstic acid/PEG 300 colloidal solution and annealed at 450, 500, and 550 °C. The latter films were obtained by six consecutive applications of the precursor, corresponding to a final thickness of ca. 2.5 μm. The data recorded for the film annealed at 400 °C are not represented in Figure 8, since the observed photocurrents were around 50 μA/cm^2. There was a significant improvement in photoactivity with increasing annealing temperature of the WO_3 films from 450 to 550 °C. However, there was no further change of the photocurrent−voltage characteristic for the film annealed at 600 °C. Inspection of scanning electron micrographs of the above films in Figure

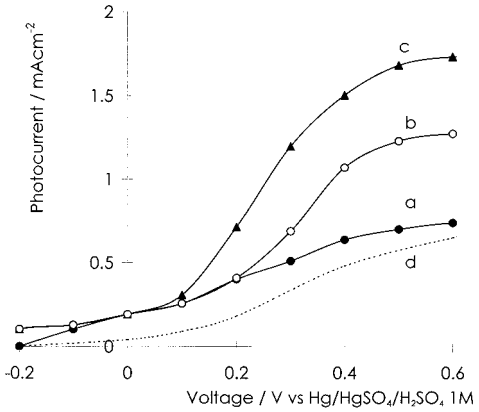

Figure 9. Effect of the annealing temperature upon photocurrent−voltage characteristics of ca. 2.5 μm thick WO_3 films prepared using tungstic acid/PEG 300 colloidal solution. The films were irradiated with simulated AM 1.5 solar light in 1 M aqueous $HClO_4$. Curves a, b, and c are for samples annealed, respectively, at 450, 500, and 550 °C. Curve d was recorded using a WO_3 film deposited in the absence of any organic additive, annealed at 550 °C.

5 might suggest marked differences observed in their porosity as a possible reason for the varying photoactivity. In fact, it is well established that the internal surface area of dye-sensitized semiconductor electrodes affects critically their conversion efficiency. However, in the present case, in view of the measurements performed with a WO_3 film annealed at 400 °C for 10 h, the porosity does not appear as the dominant factor. Despite its apparently porous structure (cf. Figure 5B), the photoactivity of the latter film remained poor, with the maximum photocurrent around 50 μA/cm^2.

Another important feature of the WO_3 films changing as a function of the annealing temperature is their crystallinity. It is to be recalled, in this connection, that the bands characteristic of the crystalline WO_3 were absent from the Raman spectrum of the sample annealed at 400 °C. This is consistent with low intensity of the XRD peaks attributable to the monoclinic WO_3 shown in Figure 7A. The development of sharp, intense diffraction peaks, starting after the heat treatment at 450 °C (Figure 7B), and culminating in an XRD pattern typical of preferentially orientated monoclinic WO_3 for the sample annealed at 550 °C Figure 7C), is, in fact, paralleled by an important increase of the photoactivity. The differing crystallinity may also be evoked to explain relatively poor photocurrent−voltage characteristics of various samples deposited using the colloidal solution of tungstic acid without any organic additive (Figure 9, curve D). This highly porous film annealed at 550 °C exhibits, in fact, the cubic structure. However, the relatively large size of the corresponding particles (cf. Figure 4) and the nature of the interparticle contacts can be also expected to affect the photoresponse. The maximum photocurrent obtained with the latter photoanodes under the simulated AM 1.5 illumination did not exceed one-third of that for the WO_3 film composed of the preferentially orientated monoclinic nanocrystallites.

Several previous reports already established a clear correlation between the crystal structure of colloidal/particulate semiconductors (Fe_2O_3,[26] WO_3,[27] TiO_2,[28]) and their photocatalytic activity. In particular, the authors of an extensive study involving a series of iron oxide polymorphs[26] point at the surface and crystal structure rather than the size and surface area of the investigated colloids as the main features affecting their activity

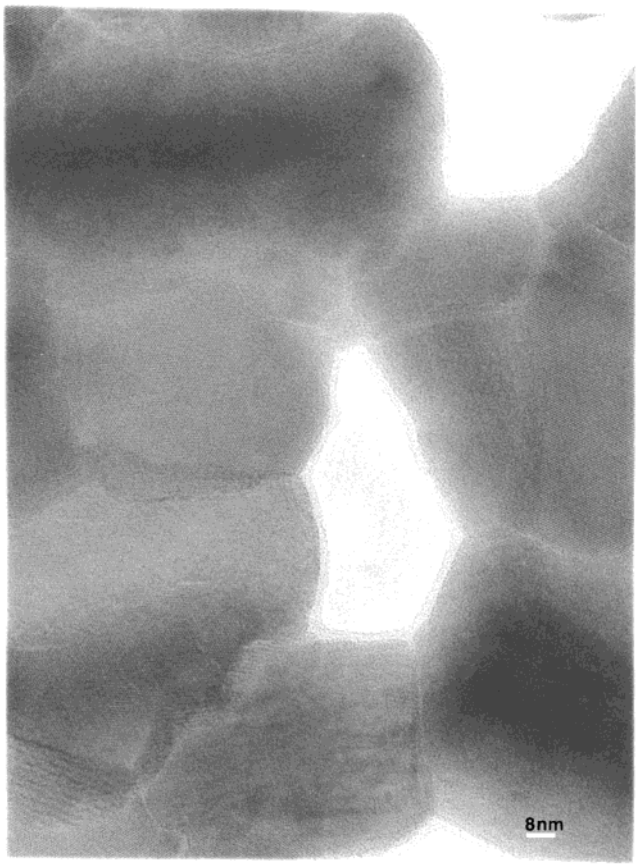

Figure 10. High-resolution transmission electron micrograph of a WO_3 nanoparticulate film (monoclinic phase) annealed at 550 °C.

in photoinduced oxidation reactions. Our own results suggest that a similar conclusion also applies to the nanostructured WO_3 films.

There exists, however, a major difference between the way in which a photooxidation reaction takes place in a suspension of colloidal semiconductor (sc) particles, respectively, and at a nanostructured sc film electrode. In fact, in the former case, the photogenerated electrons react with an appropriate acceptor from the solution while, in the second case, the electrons have to be transported to the back contact, where they are extracted as a photocurrent. Therefore, the efficient operation of such a photoanode relies also on the electron transport properties of the network of sc nanoparticles. The latter features are particularly sensitive to the crystal structure of the material and to the nature of the grain boundaries.[29] In this regard, the essentially crystalline structure of the boundaries between the nanocrystals forming the preferentially orientated monoclinic WO_3 film, revealed by images from high-resolution transmission electron microscopy (HRTEM) study (cf. Figure 10), contributes certainly to its excellent photoelectrochemical behavior.

The latter can be appreciated by inspecting incident photon-to-current-conversion efficiency (IPCE) vs excitation wavelength plot for a typical WO_3 film, polarized ca. 0.6 V above the corresponding photocurrent onset potential, shown in Figure 11.

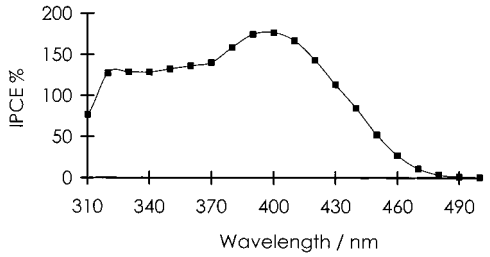

Figure 11. Photocurrent action spectrum (i.e., incident photon-to-current conversion efficiencies vs wavelength plot) for a ca. 2.5 μm thick WO_3 film, recorded in 0.1 M CH_3OH/1 M $HClO_4$ solution.

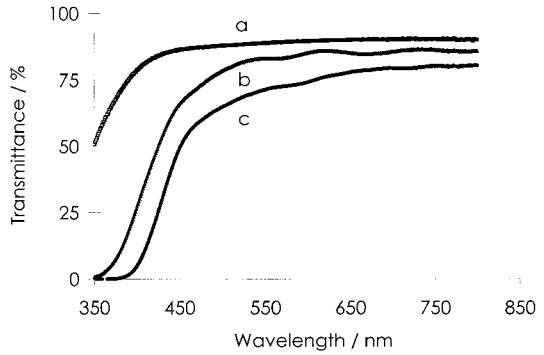

Figure 12. Total transmittance spectra of nanocrystalline WO_3 films deposited onto fused silica substrates. Curves a, b, and c are for the films having approximate thicknesses of 0.4, 1.2, and 2.5 μm.

Due to its photoresponse extending up to 500 nm and reaching a maximum around 400 nm, the WO_3 photoanode covers a significant part of the most intense region of the solar spectrum. An additional advantage of the WO_3 photoanode lies in particularly large IPCE values,[30] indicative of a low extent of electron/hole recombination, contributing to significant saturation photocurrents (up to 5 mA/cm^2) attained under the simulated solar AM 1.5 irradiation.

In Figure 12 are represented transmission spectra of three WO_3 films consisting of one, three, and six layers deposited sequentially on fused silica substrates. The spectra were recorded in the wavelength range between 350 and 800 nm. The thinnest of the films, which is representative of the samples suitable for electrochromic applications, exhibits a high degree of transmission close to 90% at 600 nm. The transmittance remains still relatively high (ca. 75% at 600 nm) for the thickest (ca. 2.5 μm thick) WO_3 film employed typically as the photoanode. Apparently, the nanostructured WO_3 films with thicknesses in the 2−3 μm range offer a good compromise between the absorption of light with energies larger than the band gap, i.e., below 500 nm, and the transparency to a large part of the visible spectrum required for the tandem cell operation.

Electrochromism. To evaluate their electrochromic aptitudes, the nanocrystalline WO_3 films were submitted to prolonged voltammetric cycling both in an aqueous solution of H_2SO_4 and in a solution of $LiClO_4$ in propylene carbonate. For these experiments we chosen highly transparent ca. 0.8 μm thick films. The cycling performed over ca. 1 V potential range corresponding to the coloration/bleaching of the films (cf. Figure 13A,B) demonstrated stable performance of the films during 10 000 cycles. The coloration efficiency (i.e., the change in optical density divided by the intercalated charge) of the films annealed at different temperatures was measured in aqueous solution.[31]

(26) Leland, J. K.; Bard, A. J. *J. Phys. Chem.* **1987**, *91*, 5076.
(27) Léaustic, A.; Babonneau, F.; Chemseddine, A.; Livage, J. *New J. Chem.* **1989**, *13*, 111.
(28) (a) Augugliaro, V.; Palmisano, L.; Sclafani, A.; Minero, C.; Pelizzetti, E. *Toxicol. Environ. Chem.* **1988**, *16*, 89. (b) Okamoto, K.; Yamamoto, A.; Tanaka, H.; Itaya, A. *Bull. Chem. Soc. Jpn.* **1985**, *58*, 2015.
(29) (a) Orton, J. W.; Powell, M. J. *Rep. Prog. Phys.* **1980**, *43*, 1263. (b) Tang, H.; Prasad, K.; Sanjinés, R.; Schmid, P. E.; Levy, F. *J. Appl. Phys.* **1994**, *75*, 2042.

(30) IPCE values larger than 100% are due to the occurrence of the photocurrent doubling characterizing photooxidation of several organic molecules (see refs 9v and 13 therein).

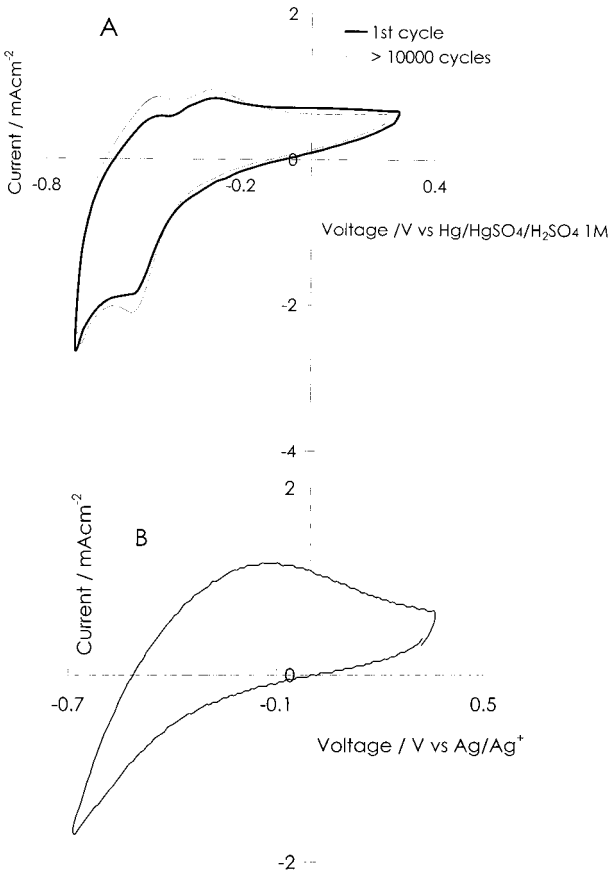

Figure 13. Cyclic voltammograms of a ca. 0.8 μm thick WO_3 film recorded at 50 mV/s in (A) 1 M aqueous H_2SO_4 and (B) 1 M $LiClO_4$ in propylene carbonate.

The highest values (ca. 40 cm^2/C) were shown by the films annealed at 500 °C.

Conclusions

We have synthesized highly transparent, nanocrystalline WO_3 films by a novel sol−gel procedure involving the use of a colloidal solution of tungstic acid stabilized by an organic additive such as poly(ethylene glycol) 300. The developed sequential deposition/annealing method allows one to build up smooth, crystallographically orientated WO_3 films in the range of thicknesses from a few hundred nanometers to a few micrometers. The size of the nanoparticles and the film porosity can be tailored by the choice of the appropriate tungstic acid/organic additive ratio and of the annealing conditions. We have established a clear correlation between the crystallinity of the WO_3 films and their photoactivity. The fully crystallized monoclinic WO_3 films exhibit the best photoresponse to the blue region of the solar spectrum (up to 500 nm). These photoanodes have been shown to maintain, under simulated solar irradiation, relatively large photocurrent densities for the photooxidation of water and, especially, that of various organic substances (reaching in the latter case 5 mA/cm^2).

Thin (less than 1 μm thick) nanocrystalline WO_3 films combine a number of features (excellent adherence and mechanical stability, open mesoporous structure, good transparency), making them promising candidates for electrochromic device applications. Preliminary measurements have shown a good degree of electrochromic optical modulation both under lithium and hydrogen ion intercalation in the films.

Acknowledgment. C.S. expresses her special thanks to John Turner for the arrangement of her stay at N.R.E.L. (Golden, CO). The authors are indebdted to Ramesh Dhere and Helio Moutinho from N.R.E.L. (Golden, CO) for their assistance in UV−vis and AFM measurements; Valery Skhlover from the Laboratory of Crystallography at ETH-Zürich (Switzerland) for his help with XRD, SEM, and TEM measurements; Anke Weidenkaff from University of Augsburg (Germany) for the valuable discussions concerning TEM results; and Jean-Pierre Rivera from the Department of Chemistry, University of Geneva (Switzerland), and Stephen M. Elliott at Thin Film Consulting (Boulder, CO) for their help in the analysis of the UV−vis spectra. This work was supported by the Swiss Federal Office of Energy and the Swiss National Science Foundation.

JA011315X

(31) Santato, C.; Augustynski, J. Manuscript in preparation.
(32) Granqvist, C. G. *Handbook of Inorganic Electrochromic Materials*; Elsevier: Amsterdam, 1995.